Design and Integration of the WCLL Tritium Extraction and Removal System into the European DEMO Tokamak Reactor

energies

MDPI

Article

Design and Integration of the WCLL Tritium Extraction and Removal System into the European DEMO Tokamak Reactor

Marco Utili [1,*], Ciro Alberghi [2], Roberto Bonifetto [3], Luigi Candido [2], Aldo Collaku [2], Belit Garcinuño [3], Michal Kordač [4], Daniele Martelli [1], Rocco Mozzillo [5], Francesca Papa [6], David Rapisarda [3], Laura Savoldi [2], Fernando R. Urgorri [3], Domenico Valerio [2] and Alessandro Venturini [1]

1 ENEA Brasimone, Camugnano, 40032 Bologna, Italy
2 Dipartimento Energia "Galileo Ferraris", Politecnico di Torino, 10129 Torino, Italy; luigi.candido@ext.f4e.europa.eu (L.C.)
3 CIEMAT-LNF, Av. Complutense 40, 28040 Madrid, Spain
4 Centrum Výzkumu Řež (CVR), Hlavní 130, 250 68 Husinec-Řež, Czech Republic
5 CREATE, Engineering School of Basilicata University, Campus Macchia, Romana, 85100 Potenza, Italy
6 DIAEE Department, Sapienza University of Rome, 00186 Rome, Italy
* Correspondence: marco.utili@enea.it

Abstract: The latest progress in the design of the water-cooled lithium–lead (WCLL) tritium extraction and removal (TER) system for the European DEMO tokamak reactor is presented. The implementation and optimization of the conceptual design of the TER system are performed in order to manage the tritium concentration in the LiPb and ancillary systems, to control the LiPb chemistry, to remove accumulated corrosion and activated products (in particular, the helium generated in the BB), to store the LiPb, to empty the BB segments, to shield the equipment due to LiPb activation, and to accommodate possible overpressure of the LiPb. The LiPb volumes in the inboard (IB) and outboard (OB) modules of the BB are separately managed due to the different pressure drops and required mass flow rates in the different plasma operational phases. Therefore, the tritium extraction is managed by 6 LiPb loops: 4 loops for the OB segments and 2 loops for the IB segments. Each one is a closed loop with forced circulation of the liquid metal through the TER and the other ancillary systems. The design presents the new CAD drawings and the integration of the TEU into the tokamak building, designed on the basis of an experimental characterization carried out for the permeator against vacuum (PAV) and gas–liquid contactor (GLC) technologies, the two most promising technologies for tritium extraction from liquid metal.

Keywords: TER; WCLL BB; DEMO; ITER; PAV; GLC

Citation: Utili, M.; Alberghi, C.; Bonifetto, R.; Candido, L.; Collaku, A.; Garcinuño, B.; Kordač, M.; Martelli, D.; Mozzillo, R.; Papa, F.; et al. Design and Integration of the WCLL Tritium Extraction and Removal System into the European DEMO Tokamak Reactor. *Energies* **2023**, *16*, 5231. https://doi.org/10.3390/en16135231

Academic Editors: Dan Gabriel Cacuci and William Martin

Received: 17 March 2023
Revised: 16 May 2023
Accepted: 19 June 2023
Published: 7 July 2023

1. Introduction

The eutectic alloy LiPb is the breeder candidate of the water-cooled lithium–lead (WCLL) breeding blanket (BB) [1], the only European driver BB candidate that uses a liquid breeder. The WCLL BB concepts used water as the coolant and the eutectic LiPb alloy (15.7 at. % Li) as the breeder and neutron multiplier. The main functions of the WCLL BB are to remove the heating power generated in the plasma; generate tritium to sustain the fusion reactions, also compensating the losses towards the environment and the other systems; and to shield the superconducting magnets. LiPb also serves the role of a tritium carrier, and the system being dedicated to the alloy's circulation through the BB to the tritium extraction unit (TEU), where tritium can be extracted from LiPb and routed to the tokamak exhaust processing (TEP) unit, is the tritium extraction and removal (TER) system. TER loops are being designed in order to manage the LiPb circulation in the reactor, to achieve an extraction efficiency rate of at least 80%, and to control the chemistry of the liquid metal. The design of LiPb loops presents several technical issues due to the characteristics of the alloy: opacity, corrosivity, a melting temperature of 235 °C, and electrical conductivity [2]. The opacity of lead alloys is a technical issue, since several measurement techniques, such as particle image velocimetry, cannot be used, meaning it is not possible to characterize the velocity profiles of lead alloys inside several components, such as the gas–liquid contactor and cold trap; therefore, it is not possible to determine the performance of the components with the traditional techniques. Moreover, the opacity of lithium lead, in combination with its high melting temperature, presents challenges related to the inspection and monitoring of major loop components. The design of the TER system is analyzed in Section 2, while in Section 3 the candidate technologies for the TEU are analyzed and the designs are compared. The design is based on numerical models developed and experimental characterizations carried out on dedicated mock-ups. The systems devoted to removing the corrosion products, activated products, and helium from the liquid metal are analyzed in Section 4, while Section 5 discusses the design of the LiPb pumping system and its integration into the LiPb loop. Finally, the whole TER integration process in the tokamak building is shown in Section 6.

2. TER Design

The implementation and optimization of the conceptual design of the TER were performed considering the main functional requirement to extract the tritium produced in the breeding modules from LiPb [3]; moreover, the TER system has to satisfy the following requirements:

1. Circulate the liquid LiPb through the BB;
2. Provide adequate heating in order to maintain the LiPb liquid in all system locations, including the BB during outgassing and baking;
3. Control the LiPb chemistry and remove accumulated activated impurities (in particular, the problem of helium generated in the BB and the necessity of discharging it using the buffer tank);
4. Ensure gravitational draining of the BB modules and LiPb loops;
5. Accommodate possible overpressure of the liquid metal.

The LiPb volumes in the inboard and outboard modules of the breeding blanket are managed separately due to the different pressure drops and required mass flow rates during operation and in the different plasma operation phases. Considering the WCLL BB segmentation in 16 sectors and the total mass flow rate for the inboard and outboard modules (Table 1), 6 LiPb loops are foreseen, namely 4 loops for the outboard (OB) segments, so that one loop is connected to 4 OB sectors, and 2 loops for the inboard (IB) segments, so that one loop is connected to 8 IB sectors. The IB and OB LiPb loops are connected to the WCLL BB [1], to the tritium plant, and to the storage tank, which is used to store all of the LiPb. Table 1 reports the main parameters for the TER loops.

Table 1. Operating conditions of IB and OB TER loops.

Parameter	OB	IB
Total mass flow rate (kg/s)	1.127	499
Number of loops (-)	4	2
Loop mass flow rate (kg/s)	281.7	249.3
Tritium concentration, c_T (mol/m^3)	1.41×10^{-2}	1.41×10^{-2}
Total LiPb inventory per loop (m^3)	164.3	154.3
LiPb inventory in BB per loop (m^3)	144.2	137.6
Total pressure drops (MPa) (including MHD)	1.82	2.6
TEU target efficiency, η (%)	≥80	≥80
Temperature, T (°C)	330	330

Each loop is a closed loop with forced circulation of the LiPb. The total amount of LiPb for each loop is about 150 m^3 and it is stored in a dedicated storage tank (TA002) during

Each loop is a closed loop with forced circulation of the LiPb. The total amount of LiPb for each loop is about 150 m³ and it is stored in a dedicated storage tank (TA002) during the non-operational phases. The tank is placed in the lowest part of the circuit in order to allow drainage by gravity (Figure 1). The LiPb is charged by a loading pump (PS004). Each TER loop is connected to the shared storage tank.

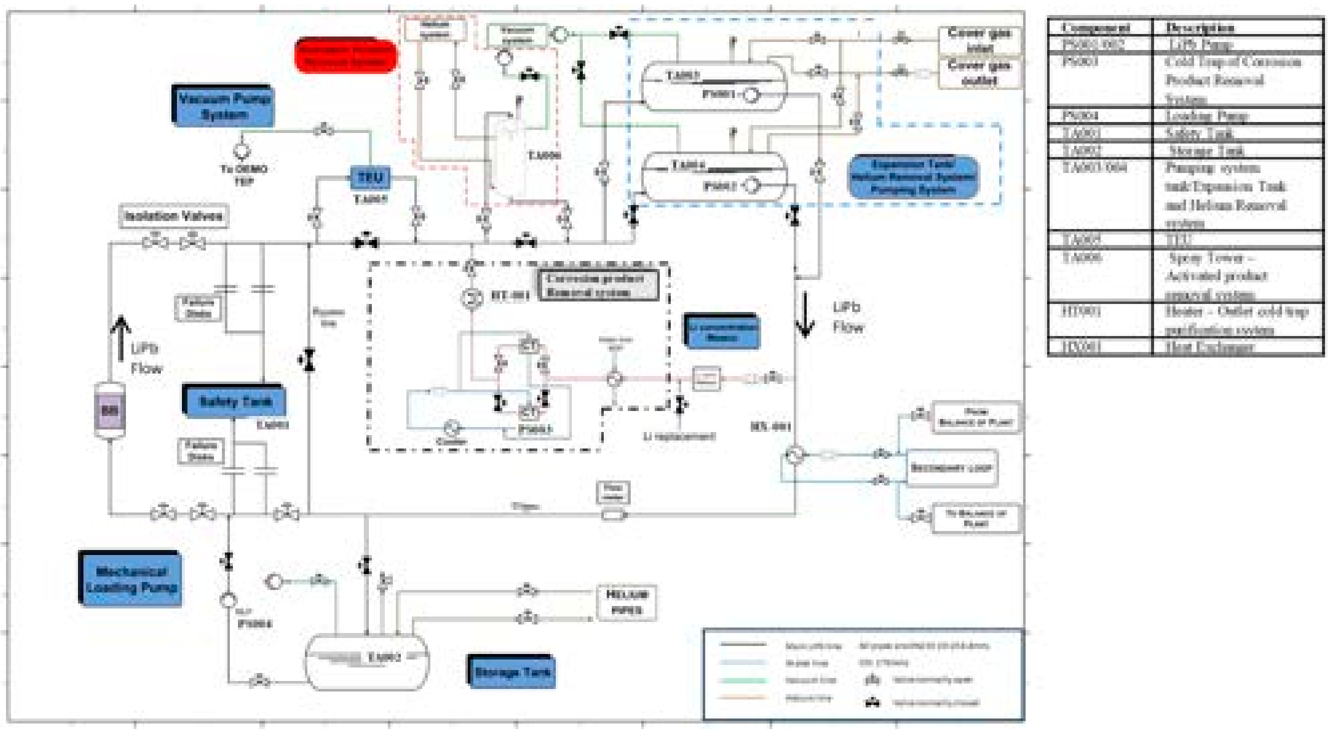

Figure 1. Layout of one TER loop. The black valves are closed during the operational phase, while the white ones are open.

In the layout shown in Figure 1, during the normal operation of the loop, the LiPb returns from the BB to the system, passes through isolation valves, and enters into the TEU. The LiPb mass flow rate managed by the TEU (TA005) corresponds to 100% of the total mass flow rate in order to reduce as much as possible the tritium inventory in the loop, and a by-pass line was installed in order to isolate the TEU from the LiPb loop during the maintenance of the system. Two LiPb pumping systems are planned for redundancy in case of the failure of one pumping station but only one will work during standard operation. The LiPb mechanical pumps (PS001/PS002) are included in the buffer tanks (TA003/TA004) in order to compensate for the thermal expansion of the LiPb and to allow for the release of helium generated inside the BB. The TEU is placed before the pumping station. From the preliminary analysis, it seems necessary that all of the LiPb passes through the buffer tank in order to ensure the discharge the helium bubbles generated in the LiPb.

After the pump, 1–10% of the alloy is sent to the corrosion product purification system (PS003), which is placed on a by-pass line of the pumping system. Instead, the system used to remove the activated products (TA006) is based on spray tower technology and is placed before the expansion tank. The adjustment of the LiPb flow will be performed by means of a regulation valve.

Then, the LiPb passes through the heat exchanger (HX001). The LiPb loops should be isothermal, although in the case that the coolant system is not able to control the LiPb temperature in the BB with high accuracy (±10 °C), a heat exchanger is needed to keep the temperature of the loop at 330 °C.

The LiPb will be recovered in the dedicated storage tank during the non-operational phases. In cases of In-box BB LOCA, due to the failure of a double-walled tube in which water flows and the consequent injection of water at about 330 °C and 155 bar in the LiPb loop [1], dedicated passive failure disks allow the fast discharge of the pressure in the safety tank, while the active isolation valves stop the water injection in the loop and the propagation of the water–LiPb mixture into the LiPb loop.

The identified TER operational phases are:

- Conditioning, constituted by baking, tritium outgassing, and vacuum conditioning;
- Plasma operation (POS), constituted by the operational state and hot standby;
- Short-term maintenance, constituted by cold standby and maintenance of the equipment, components, or pipes as a consequence of failures or as routine maintenance;
- Long-term maintenance, where the LiPb is evacuated into the storage tanks.

During the baking, carried out in the first start-up of the loops and after long-term maintenance, it is necessary to remove the impurities and oxygen solubilized in the pipes and in the equipment by heating the loops to 270–300 °C under inert atmosphere and then by pumping the vacuum in the loops and in the BB modules (0.01–1 Pa). The heating will be performed under an inert atmosphere and by using heating cables and bands for the loops, while the BB can be heated using the water cooling system. The LiPb loading is carried out under vacuum conditions to remove all of the gas from the LiPb loops and the BB.

3. TEU

Two technologies are currently considered as the most promising for tritium extraction from LiPb, the gas–liquid contactor and permeator against vacuum (PAV) technologies. In the GLC, a flow of helium (or helium plus a small percentage of hydrogen, a mix that increases the extraction efficiency) is put into direct contact with LiPb in a counter-current and the tritium is removed by the stripping gas.

Packed columns are used to provide a large interfacial surface between the LiPb and the gas flow. Instead, in the permeator against vacuum (PAV) system [1,3] a membrane separates the LiPb from the vacuum. The membrane is made with a tritium-permeable material, such as α-iron [4], vanadium, or niobium, allowing the diffusion of tritium from LiPb to vacuum as a consequence of the concentration gradient. A third promising technology is under evaluation for the extraction of tritium from the liquid metal, the liquid–vacuum contactor (LVC). In the LVC's conceptual design, the LiPb is brought into contact with a high- or ultra-high vacuum in order to enhance the diffusive process of T solubilized in the liquid metal towards the vacuum. The recent numerical and experimental studies carried out by University of Kyoto demonstrate the possibility to scale up the system [5,6] with high efficiency. Preliminary designs of TEUs based on PAV, GLC, and LVC technologies with a minimum tritium extraction efficiency of 80% are carried out on the basis of the experimental results obtained from prototypical mock-ups installed in the TRIEX-II [7,8] and CLIPPER facilities. The designs of the manufactured and qualified mock-ups are analyzed in the following paragraphs.

The LiPb properties adopted in the analysis are reported in Table 2 with the corresponding references.

Table 2. LiPb properties.

Parameter	Value	Ref
Sievert's constant, K_s (mol $Pa^{-0.5}$ m^{-3})	$2.37 \times 10^{-1} \cdot \exp(-12{,}844/RT)$	[9]
Diffusivity, D (m^2 s^{-1})	$4.03 \times 10^{-8} \cdot \exp(-19{,}500/RT)$	[10]
Mass transfer coefficient, K_t (m s^{-1})	$2.50 \times 10^{-3} \cdot \exp(-30{,}700/RT)$	[11]
Recombination constant, K_r (m^4 mol^{-1} s^{-1})	$5.73 \times 10^{-2} \cdot \exp(-29{,}717/RT)$	[12]
Density, ρ (kg m^{-3})	$10{,}520.35 - 1.19051 \cdot T$	[2]

3.1. PAV

This technique consists of tritium's permeation from the LiPb through a membrane containing the liquid metal to a secondary chamber subjected to a vacuum. The driving force is the pressure gradient generated by the vacuum onto the external surface of the membrane [13]. One of the key points to improve the process is the use of highly permeable

3.1. PAV

This technique consists of tritium's permeation from the LiPb through a membrane containing the liquid metal to a secondary chamber subjected to a vacuum. The driving force is the pressure gradient generated by the vacuum onto the external surface of the membrane [13]. One of the key points to improve the process is the use of highly permeable materials for the membrane. Additionally, there should be chemical compatibility with the liquid LiPb alloy to avoid corrosion and malfunctions. For this, last years' research program was focused on the PAV's development using vanadium and niobium as the membrane materials [7]. Within the European program, two main geometries are being tested: one based on rectangular flat channels for LiPb flows using vanadium plates [14] and the other one based on a tubular arrangement of niobium pipes [15].

3.1.1. PAV Design Based on Nb Tubes

One of the designs is constituted by permeable niobium tubes inside a vacuum vessel. Each vessel is a cylinder assumed to be installed vertically in the tokamak building. Each vessel contains the channels for the LiPb flow: the niobium wall of the pipes is the tritium permeation membrane. The parallel channels are "U-shaped", as reported in [16] and shown in Figure 2. Three manifolds are present in the bottom of the vessel, where the LiPb is collected at the inlet section in a manifold, then passes through a first set of U-pipes, reaching an intermediate manifold. From the latter and through a second set of U-pipes, the LiPb flows to the outlet manifold. Before loading the LiPb in the PAV, vacuum is pumped inside the Nb pipes in order to remove the gas and allow LiPb charging.

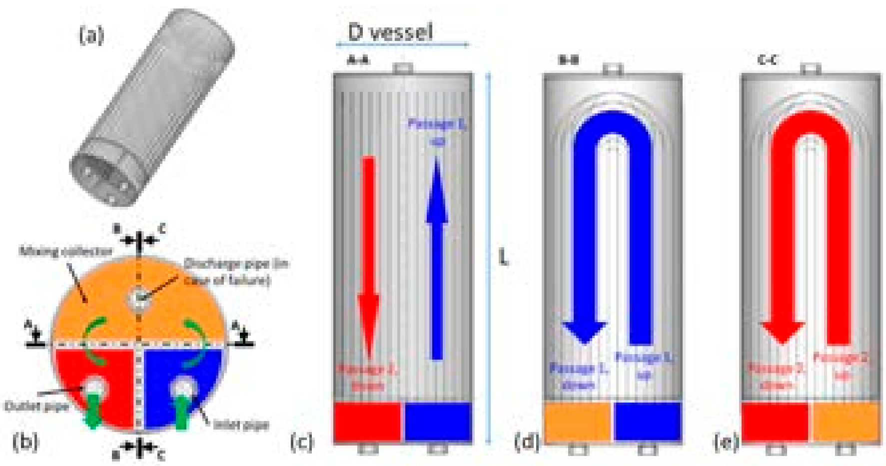

Figure 2. View of the TEU design based on a PAV: (**a**) 3D view, vessel internals; (**b**) top view with the inlet, outlet, and discharge pipes shown transparently; (**c**) side view with inlet and outlet manifolds; side views of passages 1 (**d**) and 2 (**e**).

Thanks to the permeation properties of the niobium and the tritium's partial pressure gradient across the membrane, the tritium dissolved in the LiPb is extracted by the vacuum circuit. Therefore, while running along the U-pipes, the LiPb reduces its tritium concentration.

As described in detail in [15], the main constraints for the PAV dimensioning concern the space occupation (limited by the space allocated for its installation in the plant, allowing a vessel diameter of up to 7 m) and the allowable pressure drop (about 2 bar). The maximum permeator length (40 m) is related to the maximum height of the vessel (10 m) and the fact that there are 2 U-pipe passages.

The dimensioning of the PAV was carried out for one of the OB loops, as they feature the largest mass flow rate (up to 264 kg/s), varying the following parameters:

- Geometry (vessel diameter, pipe number, diameter, and length);
- Operating temperature (from 330 C to 500 °C);
- Permeation regime (diffusion- or surface-limited, mainly depending on the real membrane permeation properties, also connected to the oxidation status of its surface).

The operating conditions and constraints retained for the design are reported in Table 3.

Table 3. Design parameters adopted in designing a PAV for DEMO and the design constraints.

Design Parameters (Operating Conditions)	Value
Tritium partial pressure (@ PAV inlet)	55 Pa
Membrane thickness	0.4 mm
Pipe internal diameter	9.2 mm
Design Constraints	
Maximum overall height of PAV	10 m
Maximum allowable pressure drop	0.2 Mpa
Efficiency	80%
Min/max velocity in the pipes	0.21–2.1 m/s

As shown in [16], it is possible to operate the OB TEU featuring the PAV technology with the Nb membrane with an extraction efficiency of 90%:

- At any temperature, including the operating temperature of 330 °C, in the diffusion-limited regime (non-oxidized surface) or in the surface-limited regime but considering a series connection of at least two permeators and a reduction to 70% of the target extraction efficiency;
- At 400 °C in the surface-limited regime but considering a series connection of at least two permeators (or a reduction to 70% of the target extraction efficiency);
- At 500 °C in the surface-limited regime.

PAV sizing was carried out at the LiPb outlet temperature (330 °C). The superficial status of the membrane material determines the tritium transport regime and the PAV sizing, and a few oxide layers on the surface can change the Nb or V permeability value by one order of magnitude. The design was carried out on the basis of the experimental characterization of niobium and vanadium's permeability performed in two independent laboratories [7] and by the characterization in flowing LiPb in the TRIEX-II facility of the PAV mock-up [15] (Figure 3), called PAV-ONE. The mock-up is constituted by 16 Nb tubes, characterized by a length of 2 m, a diameter of 4 mm, and a thickness of 0.2 mm. The Nb tubes' thickness was selected based on the certified Nb pipes available on the market with a length of 2.00 m and closest to the Nb pipe thickness selected for DEMO. The TRIEX-II (tritium extraction) facility was manufactured and installed at ENEA C.R. Brasimone with the objective of characterizing the different candidate technologies as the tritium extraction unit (TEU) of the ITER WCLL-TBM and DEMO WCLL-BB. We were capable of qualifying three kinds of extractor mock-ups—the GLC, in the packed column configuration, the PAV, and even the LVC. The mock-ups were tested in the TRIEX-II facility in flowing LiPb and using protium (or deuterium) as a substitute for tritium for safety reasons. A chromium–molybdenum steel (ASTM A335 Gr. P22) is used as the structural material at TRIEX-II due to its low corrosion rate linked with the low nickel concentration [17]. More details on the TRIEX-II facility can be found in [7]. The experimental PAV-ONE characterization process was carried out with LiPb and solubilized hydrogen, whereby the LiPb flowed inside the POV-ONE tubes with a total mass flow rate in the range between 0.6 and 1.2 kg/s and the hydrogen that permeated through the pipes was monitored by a mass spectrometer in order to detect the permeated flux. PAV-ONE was characterized at the temperatures of 350 °C and 450 °C and in the hydrogen partial pressure range of LiPb of between 100 and 400 Pa.

The TEU designed for the OB loop required in the surface-limited tritium transport analysis 1600 Nb tubes, while instead in the diffusion-limited regime the number of tubes is reduced to 855, Table 4. For the diffusion-limited regime, it is expected that with cleaned Nb pipes, a thin oxide layer can reduce the permeation flux by a factor 1000; therefore, the measure of the Nb permeability under relevant operating conditions is mandatory to design the TER system based on PAV technology.

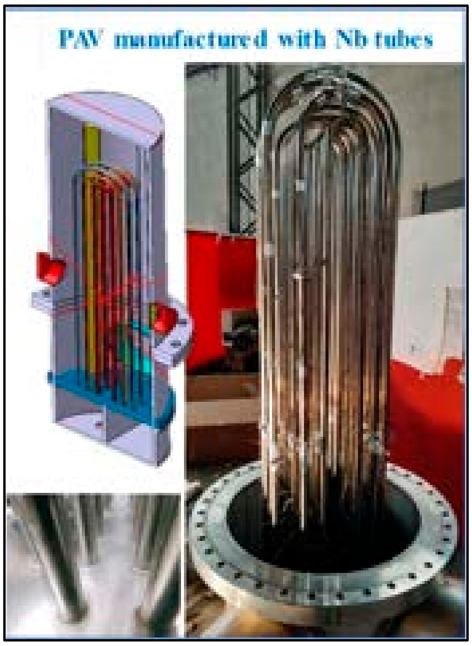

Figure 3. PAV-ONE mock-up installed in the TRIEX-II facility and details of the Nb tubes.

Table 4. OB PAV design calculated under the diffusion-limited regime (cleaned Nb pipes) and surface-limited regime (permeability measured with related cleaning conditions).

OB PAV Design Parameters	Value in Surface-Limited Regime (Oxidized Surface)	Value in Diffusion-Limited Regime (Non-Oxidized Surface)
Efficiency	92%	92%
LiPb temperature (°C)	330 °C	330 °C
Pressure drops (MPa)	<0.3	0.066
Vessel diameter (m)	6	4
Height of tank (m)	8	6
No. of Nb tubes	1600	855
Diameter Nb tube (mm)	9.2	9.2
Length Nb Tube (m)	57	27.75
Total interface area Nb/LiPb (m^2)	3723	968
Nb permeability at 330 °C (mol/m s $Pa^{0.5}$)	4.8×10^{-13} [18]	9.27×10^{-7} [19]

A modular design approach, based on the permeation model in the diffusion-limited regime at 330 °C, was developed in order to reduce the size of each singular PAV tritium extraction modules. A modular PAV unit (PAVU) was designed, which could serve both the inboard and outboard BB loops when an appropriate number of units is suitably connected in parallel, assuming a Nb pipe diameter of 9.2 mm.

To ensure the compatibility of the module design for both the OB and IB modules, the procedure described in the flowchart in Figure 4 was developed. Following the workflow in Figure 4, it can be found that 4 or 5 PAVUs in each OB loop allows the use of a number of tubes in the PAVUs that is compatible to that obtained for each loop of the IB (see Figure 5). When 5 PAVUs per OB loop are considered, the mass flow rate in each OB PAVU is 52.8 kg/s, while it is 53 kg/s for the IB PAVU. It is shown that the set of constraints is fully satisfied for both IB and OB conditions if the number of tubes in the PAVUs is within the range of 299–385 (pipes with a diameter of 9.2 mm and length of 40 m, i.e., 2 U-tubes with a total height of 10 m).

within the range of 2… (pipes with a diameter of … and length of 40 m, i.e., 2 U-tubes with a total height of 10 m). a number of tubes in the PAVUs that is compatible to that obtained for each loop of the IB (see Figure 5). When 5 PAVUs per OB loop are considered, the mass flow rate in each OB PAVU is 52.8 kg/s, while it is 55 kg/s for the IB PAVU. It is shown that the set of constraints … tubes in the PAVUs is … length of 40 m, i.e., 2 U-

Figure 4. Flowchart adopted in the design of the PAVU (#PP is the number of tubes in the PAVU).

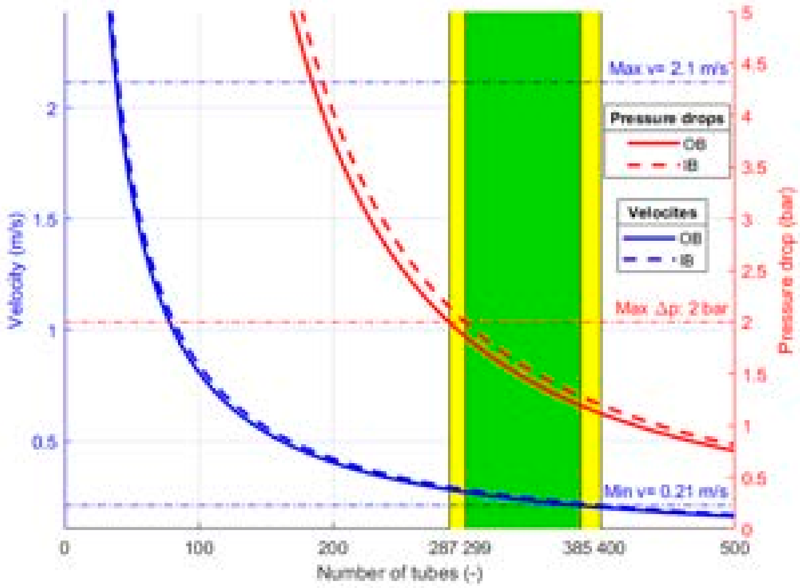

Figure 5. Results obtained with the DLR, for 5 PAVUs for each OB loop at a LiPb inlet temperature of 330 °C: the velocity (in blue, left axis) and pressure drop (in red, right axis) as a function of the number of tubes. Horizontal dashed lines represent design constraints. The number of tubes shaded in yellow refers to only one IB or OB module, while that in green refers to a range common to both.

The range of tube numbers that satisfy the constraints on the pressure drop and on the fluid velocity within a 40 m length for a mass flow rate of either one-fifth or one-quarter of the loop mass flow rate is between 360 and 385 tubes in each PAVU; the same device could fit groups of 4 or 5 units for each OB loop, and as a single unit for each IB loop, dramatically simplifying the overall design of the TEU.

3.1.2. PAV Design Based on V Plates

At CIEMAT, efforts are being devoted to the experimental validation of a vanadium-based PAV. A first prototype—TRITON—was manufactured using 1-m-long vanadium

3.1.2. PAV Design Based on V Plates

At CIEMAT, efforts are being devoted to the experimental validation of a vanadium-based PAV. A first prototype—TRITON—was manufactured using 1-m-long vanadium membranes welded to a common steel structure through TIG welding [20] (Figure 6). The poor compatibility between these dissimilar materials led to leaks in the component and to a change in the manufacturing approach. As an alternative, electron beam welding technology was selected. Although the results were promising, the final integrity of the component was compromised by the high stresses the welds were subjected to due to the length of the device (Figure 7).

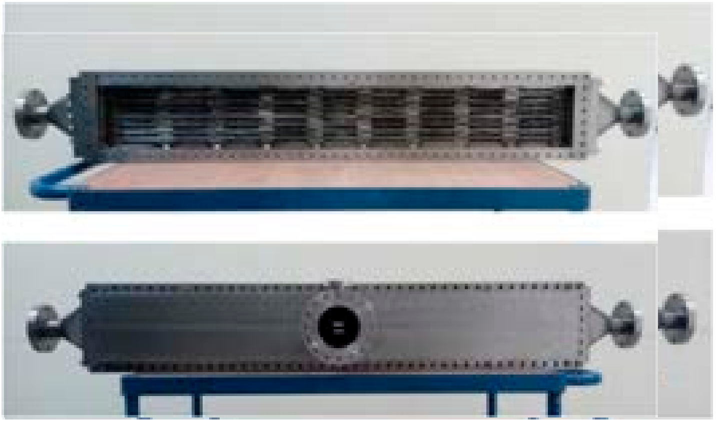

Figure 6. TRITON PAV prototype made of vanadium.

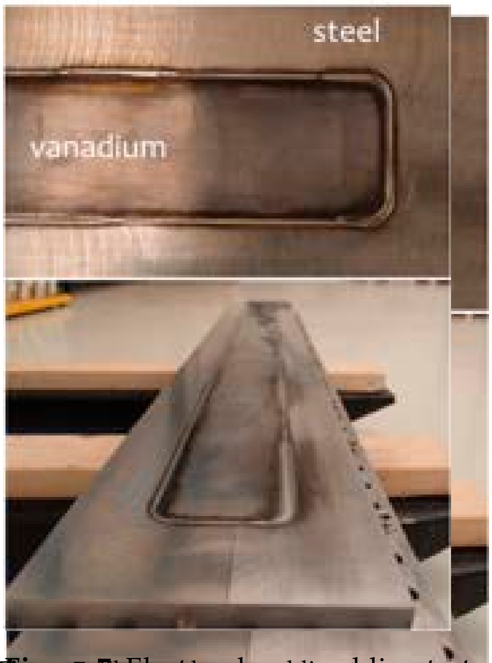

Figure 7. Electron beam welding test.

A new modular prototype was built based on a screwed attachment of vanadium by using graphite gaskets. It consists of individual vacuum boxes made of a supporting structure of AISI410, where two vanadium membranes are fixed with NOVAPHIT gaskets and screws (Figure 8). In this way, it is possible to test each vacuum channel before assembly to detect leaks. The steel structure has penetrations to connect the vacuum system and then extract the H/D gas permeated through the membrane. The LiPb loop CLIPPER (CIEMAT) [21] (Figure 9) was manufactured to host an experimental campaign for the validation of this component, which is currently ongoing. The loop has flexibility to operate under a wide range of conditions (250–550 °C, 0.4–4 L/s) and deuterium pressures [20].

to operate under a wide range of conditions (350–550 °C; 0.4–4 L/s) and deuterium pressures [20].

Figure 8. Modular PAV prototype made of vanadium.

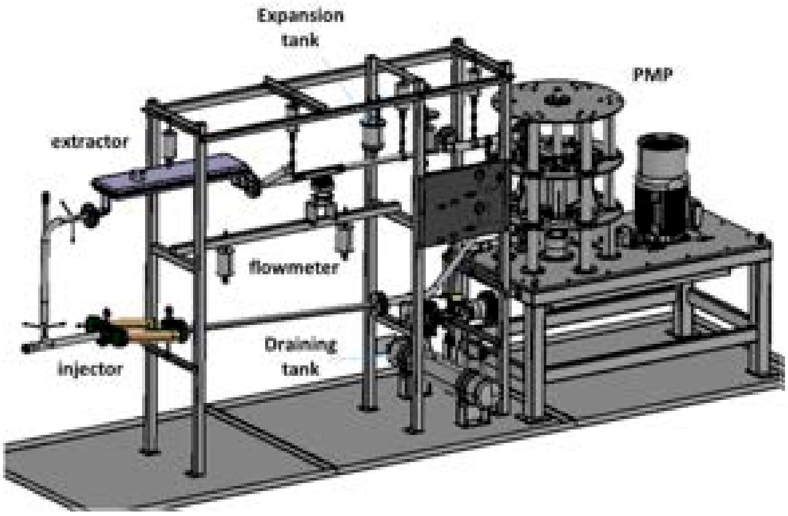

Figure 9. 3D view of the CLIPPER facility.

The experiments were firstly focused on a WCLL-relevant scenario, where theoretical simulations showed an extraction efficiency range of the mock-up of between 5 and 20%, with fluxes in the order of $7 \cdot 10^{-7}$ mol/s. For high temperatures and low flows, the extraction performance can increase by up to 40% [14].

The next step was evaluating, from a mathematical point of view, the PAV technique at the reactor scale. For this, the main WCLL parameters were used [22]. A minimum efficiency of 80% was considered [23] for a PAV design based on a rectangular configuration and with vanadium membranes [24]. The employed mathematical model is described in [14]. Taking into account that the mass flow per IB loop is 249 kg/s and per OB loop is 281 kg/s [1], two TEU designs are needed to manage the different mass flows, although there are slight differences and only OB geometrical parameters are reflected in Table 5. In view of the high surface permeation level required, a first approach for the implementation into a real TEU system could be the attachment of several membranes (maximum length of approximately 2 m) into a common base structure. Moreover, a modular approach for PAV was estimated with a mass flow rate for each module of 55 kg/s.

Number of LiPb channels 120
Total number of channels 241
LiPb velocity 2.4 × 10⁻² m/s
Total membrane area in contact with LiPb 6840 m²
Efficiency 80%
Volume of LiPb 17.10 m³
Vacuum volume 17.24 m³

Table 5. OB PAV design based on V plates.

Parameter	OB-PAV	Modular-PAV
Width	1.90 m	1.20 m
Channel height	5×10^{-3} m	5×10^{-3} m
Length	15 m	10 m
Membrane thickness	1×10^{-3} m	$1 \cdot 10^{-3}$ m
Number of LiPb channels	120	100
Total number of channels	241	201
LiPb velocity	2.4×10^{-2} m/s	9.4×10^{-3} m/s
Total membrane area in contact with LiPb	6840 m^2	2400 m^2
Efficiency	80%	
Volume of LiPb	17.10 m^3	6.00 m^3
Vacuum volume	17.24 m^3	7.06 m^3

Applying the same rationale as in [23], the pumping speed requirements for the vacuum system were evaluated. It was found that values below 0.5 m^3/s are needed if the solubility of tritium in LiPb is applied as per Reiter's method [10], whereas values of up to 371 m^3/s are required if Aiello's Ks [9] is employed.

3.2. *GLC*

3.2.1. GLC Mock-Up Characterization

Gas–liquid contactors implement well-known industrial technology [25], where a gas and a liquid are brought into contact so that diffusion exchange occurs between them (Figure 10). In particular, the packed column configuration adopted is constituted by a vertical column filled with Sulzer MellapakPlus 452Y (surface-to-volume ratio of 350 m^2/m^3) structured packing.

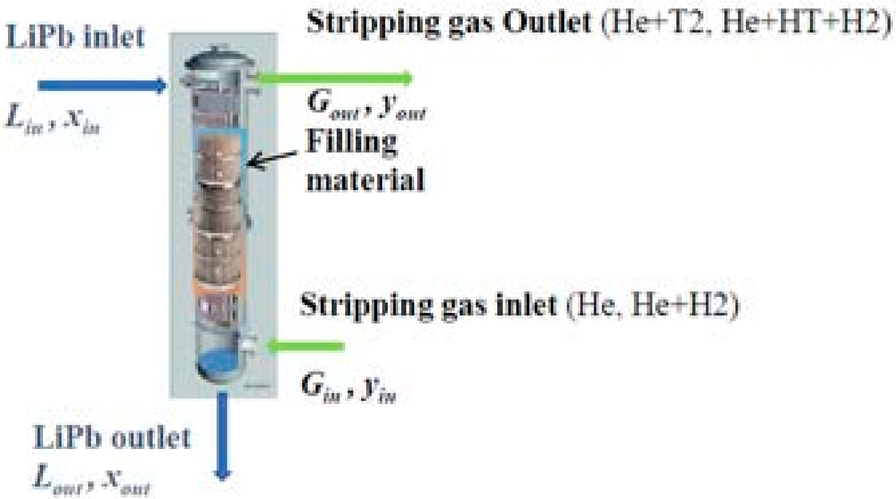

Figure 10. Sketch of the GLC extractor with the nomenclature of the efficiency calculations.

The most relevant results obtained in TRIEX-II were achieved by solubilizing deuterium in liquid LiPb and extracting it with a stripping gas of helium plus a 0.5% vol. addition of hydrogen in order to enhance the extraction efficiency. The results of the 6 tests are reported in Figure 11.

The picture shows the extraction efficiency as a function of the L/G ratio, expressed as m^3_{LiPb}/Nm^3_{gas}, i.e., the ratio between the liquid LiPb mass flow rate and the stripping gas flow rate. The former flow rate was varied in the range of 0.5–1 kg/s and the latter in the range of 25–103 Nl/h, with a LiPb temperature of 450 °C. As detailed in [7], the extraction efficiency was measured by means of a quadrupole mass spectrometer, calibrated such that the isobaric interferences were reduced as low as possible, enabling the possibility to discern D_2 from He. The maximum extraction efficiency rate of 44% was found for an

Applying the same rationale as in [23], the pumping speed … vacuum system were evaluated. It was found that values below 0.… solubility of tritium in LiPb is applied as per Reiter's method [10… to 371 m³/s are required if Aiello's Ks [9] is employed.
3.2. GLC
3.2.1. GLC Mock-Up Characterization
Gas–liquid contactors implement well-known industrial tech… and a liquid are brought into contact so that diffusion exchang… (Figure 10). In particular, the packed column configuration ado… vertical column filled with Sulzer MellapakPlus 452Y (surface-… m³/m³) structured packing.
Figure 10. Sketch of the GLC extractor with the nomenclature of the effic…
The most relevant results obtained in TRIEX-II were ac… deuterium in liquid LiPb and extracting it with a stripping gas of… addition of hydrogen in order to enhance the extraction efficien… tests are reported in Figure 11.

L/G ratio equal to 1.2 m^3_{LiPb}/Nm^3_{gas}. The data were significantly correlated, with a with a *p*-value that was remarkably lower with respect to the significance level of $\alpha = 0.05$.

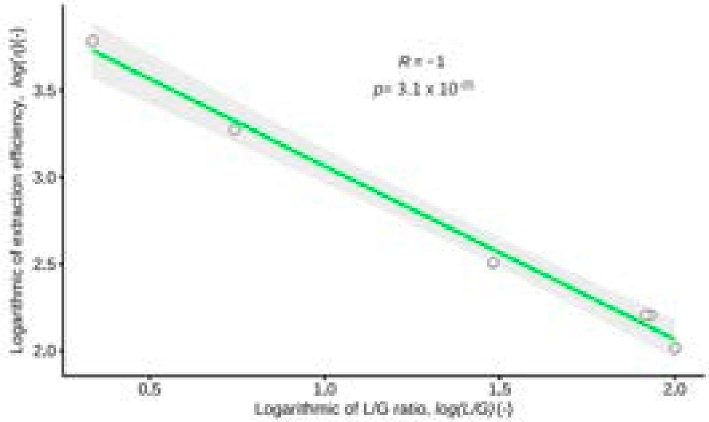

Figure 11. Pearson correlation for tests with deuterium at $T = 450$ °C.

The picture shows the extraction efficiency as a function of the L/G ratio, expressed as m^3_{LiPb}/Nm^3_{gas}, i.e., the ratio between the liquid LiPb mass flow rate and the stripping gas flow rate. The former flow rate was varied in the range of 0.5–1 kg/s and the latter in the range of 28–103 Nl/h, with a LiPb temperature of 450 °C. As detailed in [7], the extraction efficiency was measured by means of a quadrupole mass spectrometer, calibrated such that the isobaric interferences were reduced as low as possible, enabling the possibility to discern D_2 from He. The maximum extraction efficiency rate of 44% was found for an L/G ratio equal to 1.2 m^3_{LiPb}/Nm^3_{gas}. The data were significantly correlated, with a with a *p*-value that was remarkably lower with respect to the significance level of $\alpha = 0.05$.

3.2.2. GLC Design for DEMO

To meet the DEMO requirements [26], the following operating conditions were adopted in the pre-conceptual design of the GCL scale-up process (Table 6). The GLC dimensioning was carried out considering an extraction efficiency of 44%, with hydrogen added to the helium stripping gas and structured fillings with a surface-to-volume ratio spanning in the range of 125–750 m^2/m^3 (commercially available from Sulzer). The operating temperature of the column, which is supposed to be isothermal, was analyzed in the range of 330–500 °C.

Table 6. Operating conditions adopted in the GLC DEMO design.

Design Parameters	WCLL BB
L/G ratio (-)	1.4
Surface-to-volume ratio (1/m)	125–750
TES operating temperature	330–500
TES efficiency (1 module) (%)	44
TES efficiency (3–4 modules) (%)	82–90

Several sensitivity analyses were carried out in order to find the optimal configuration of the GLC for the WCLL-BB for DEMO. The analysis was carried out considering that the GLC column is constituted by several transfer units, which are the hypothetical stages needed to transfer one unit of the solute from the concentrated solution to the stripping one. The adopted procedure is reported in [7] and leads to an integral expression used to calculate the number of theoretical stages and transfer units. Since highly efficient tritium extraction systems are expected for DEMO, at least 3 units arranged in series should be foreseen for each LiPb circuit in order to provide an overall extraction efficiency of 82%.

For the evaluation of the GLC column diameter and column height for DEMO, it is possible to write:

$$HTU = HTU_{OL} = \frac{L_{mol}}{k_{LLE}\ C_t\ a\ A_c} \quad (1)$$

where HTU and HTU_{OL} are the height of the transfer unit (HTU) and the height of the overall gas and liquid transfer units, respectively (m), L_{mol} (mol/s) is the molar flow rate of LiPb, Ac (m^2) is the GLC cross-section of the column, C_t (mol/m^3) is the total concentration of the liquid, a (m^2/m^3) is the surface-to-volume ratio of the column. The active height of the column is:

$$h = S_f\ HTU\ NTU \quad (2)$$

Figure 11. Pearson correlation for tests with deuterium at $T = 450$ °C.

3.2.2. GLC Design for DEMO

To meet the DEMO requirements [26], the following operating conditions were adopted in the pre-conceptual design of the GCL scale-up process (Table 6). The GLC dimensioning was carried out considering an extraction efficiency of 44%, with hydrogen added to the helium stripping gas and structured fillings with a surface-to-volume ratio spanning in the range of 125–750 m²/m³ (commercially available from Sulzer). The operating temperature of the column, which is supposed to be isothermal, was analyzed in the range of 330–500 °C.

Table 6. Operating conditions adopted in the GLC DEMO design.

Several sensitivity analyses were carried out in order to find the optimal configuration of the GLC for the WCLL-BB for DEMO. The analysis was carried out considering that the GLC column is constituted by several transfer units, which are the hypothetical stages needed to transfer one unit of the solute from the concentrated solution to the stripping one. The adopted procedure is reported in [7] and leads to an integral expression used to calculate the number of theoretical stages and transfer units. Since highly efficient tritium extraction systems are expected for DEMO, at least 3 units arranged in series should be foreseen for each LiPb circuit in order to provide an overall extraction efficiency of 82%.

overall gas and liquid transfer units, respectively (m); L_{mol} (mol/s) is the molar flow rate of LiPb; Ac (m^2) is the cross-section of the column; C_t (mol/m^3) is the total concentration of the liquid; a (m^2/m^3) is the surface-to-volume ratio of the column. The active height of the column is:

$$h = S \cdot HTU \cdot NTU$$

For instance, in Figures 12 and 13, the theoretical height as a function of the column diameter is shown for different operating temperatures of the column. The column height decreases when increasing the operating temperature of the column, i.e., the temperature of the lithium–lead at the inlet of the TES. If the TES was operated at 500 °C, the theoretical height of one module for the OB would be 0.97 m instead of 3.64 m (330 °C). For the IB, the module height shifts from 0.76 m to 0.20 m.

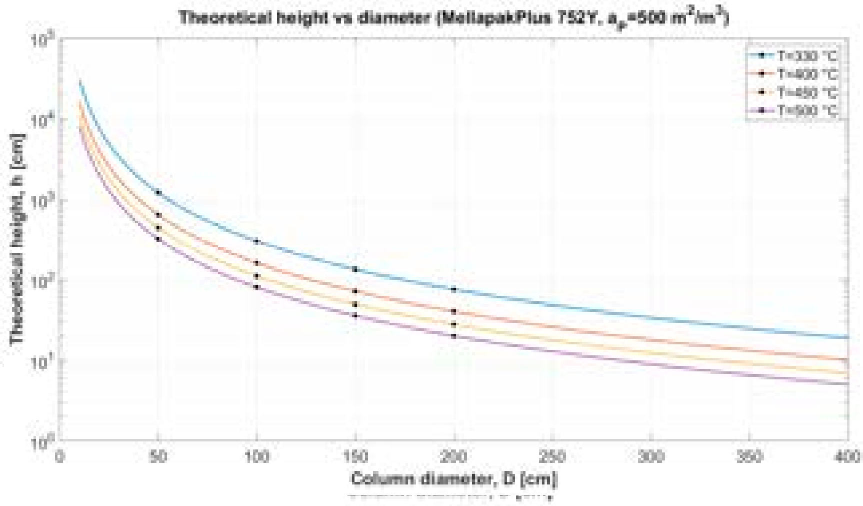

Figure 12. Sensitivity study for IB segment—sweep on operating temperature.

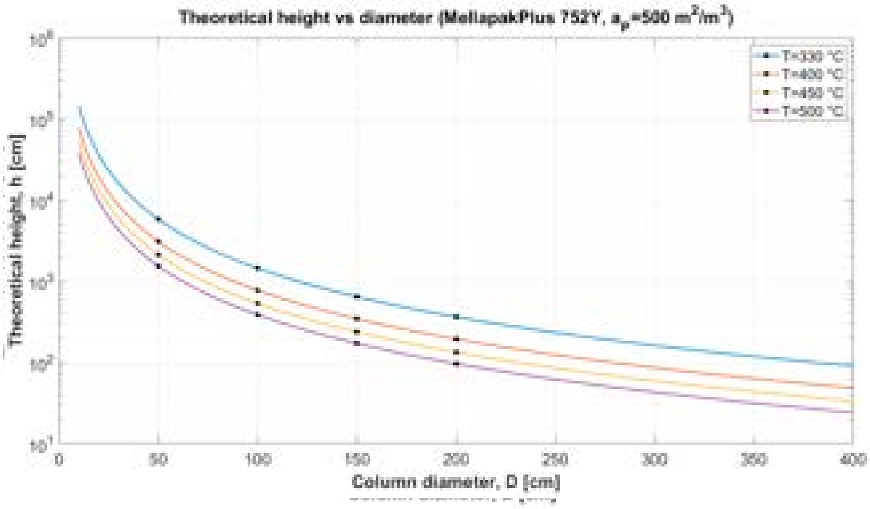

Figure 13. Sensitivity study for OB segment—sweep on operating temperature.

A possible configuration of the TER adopting the GLC technology is shown. The optimization process was carried out considering the same temperature for the IB and OB lithium–lead circuits (T = 450 °C) and a maximum column height of 10 m. The space required for the liquid and gas distributor, supports, and liquid collector was taken into account considering the parameters reported in [27]. By using the same structured filling as the one used in TRIEX-II (Mellapak 452Y), the total heights of the IB and OB columns were 4.30 m and 10.27 m, with a 2 m diameter. A TRS is required to remove tritium from the stripping gas:

- A nominal volumetric flow rate of 521 Nm^3/h required for the outboard module;
- A nominal volumetric flow rate of 108 Nm^3/h required for the inboard module.

An overview of the results obtained is reported in Table 7.

Table 7. Final parameters for the GLC scaled to DEMO.

Parameter [Unit]	OB Value	IB Value	Notes
Inlet stripping gas pressure	1.0–1.4 Mpa	1.0–1.4 Mpa	Helium plus H_2 stripping gas
Total stripping gas flow rate to TEU	400–1000 Nm^3/h	100–6000 Nm^3/h	
Stripping gas composition inlet TEU	He + H_2 0.1–0.5% mol	He + H_2 0.1–0.5% mol	
Height of the vessel	9–11 m	4–5.5 m	Preliminary estimation with surface-limited regime
External diameter of the vessel	2–3 m	2–3 m	Preliminary estimation
Outflow of HT + T_2 from TEU to TRS	56 ± 5% g/d	48 ± 5% g/d	Accounting for a 70% outboard contribution to the total tritium generation rate (320 g/d) and for the share of a single outboard LiPb loop

3.3. LVC

The liquid–vacuum contactor is the third technology analysed for the TEU design and it is considered as back-up solution due to some relevant uncertainties in the design and the lower maturity of this technology compared with the PAV and GLC. In liquid–vacuum contactors, the liquid domain is kept in direct contact with the vacuum side. The hydrogen isotope atomically solubilized in the liquid carrier migrates from the bulk to the interface between the liquid and vacuum and then it recombines to molecular hydrogen departing from the surface. Among the possible designs, the vacuum sieve tray (VST) is one of the most promising, where the interface between the LiPb and vacuum is realized with LiPb droplets. The use of VSTs is a high-efficiency and promising method to extract tritium from liquid lithium–lead alloys. The lithium–lead flows from an upper chamber to the bottom one, kept under dynamic vacuum conditions, passing through a tray equipped with nozzles of a diameter of the order of the millimeter, which allows the alloy to form an unstable liquid jet of droplets. The atoms of hydrogen isotope Q are transported from the inside of the falling droplets to their outer surface, where they recombine to form Q_2, which leaves the liquid metal and is collected using a vacuum pump train. Extended R&D activities on VST extractor systems have been performed at Kyoto University in Japan [5,6]. Another configuration of the liquid–vacuum contactor is given by the free surface extractor. In this system., the liquid flows in a channel where there is direct contact between the whole surface of the liquid phase and the vacuum. Tritium migrates from the liquid towards the vacuum and is collected by a vacuum pumping system.

3.3.1. Analysis of the Advantages of the Use of Membrane Materials with Respect to the Direct LVC

In order to analyse whether the tritium extraction from LiPb is more efficient with direct contact between the LiPb and vacuum or with an interposed permeable membrane, an experiment is being prepared at CIEMAT. The test will determine whether the membrane acts as a true 'catalyzer' of the permeation process, enhancing the extraction of H-isotopes from the liquid metal. For this, two extractors are being manufactured: one with a vanadium membrane (PAV prototype) and the other with flowing LiPb directly exposed to vacuum conditions (free surface LVC prototype) (Figure 14). The comparison between both approaches will be performed in a dedicated experimental campaign in CLIPPER (Figure 9), and under WCLL-relevant conditions [28,29]. The main design requirements are having the same effective permeation surface, the same operational conditions, and the need to reach a steady state to compare results. A system with a 1 m length of exposed surface or membrane could provide a flux of 1×10^{-8} mol/s, which is enough for its detection. Figure 15 shows the steady-state extraction flux and the extraction efficiency as a function of the mass flow rate in CLIPPER for both methodologies. These were computed using a 1D system level approach and empirical correlations for the mass transfer coefficient [29]. The calculations were performed with the experimental vanadium permeability obtained at CIEMAT [19,30]. Despite the prototype being expected to work at low efficiency rates, extraction efficiency as a function of the mass flow rate in CLIPPER for ... methodologies. These were computed using a 1D system level approach and empirical correlations for the mass transfer coefficient [29]. The calculations were performed using the experimental vanadium permeability obtained at CIEMAT [19,30]. Despite the prototype being expected to work at low efficiency rates, the modelling confirmed that the expected steady-state fluxes in the CLIPPER facility are between the detection limits of the measurement system.

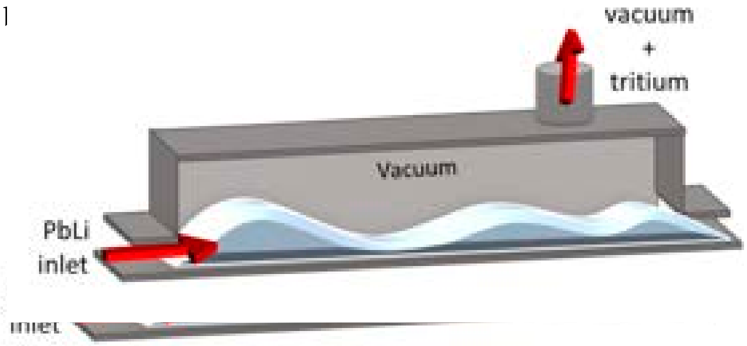

Figure 14. Scheme of the free surface extractor prototype.

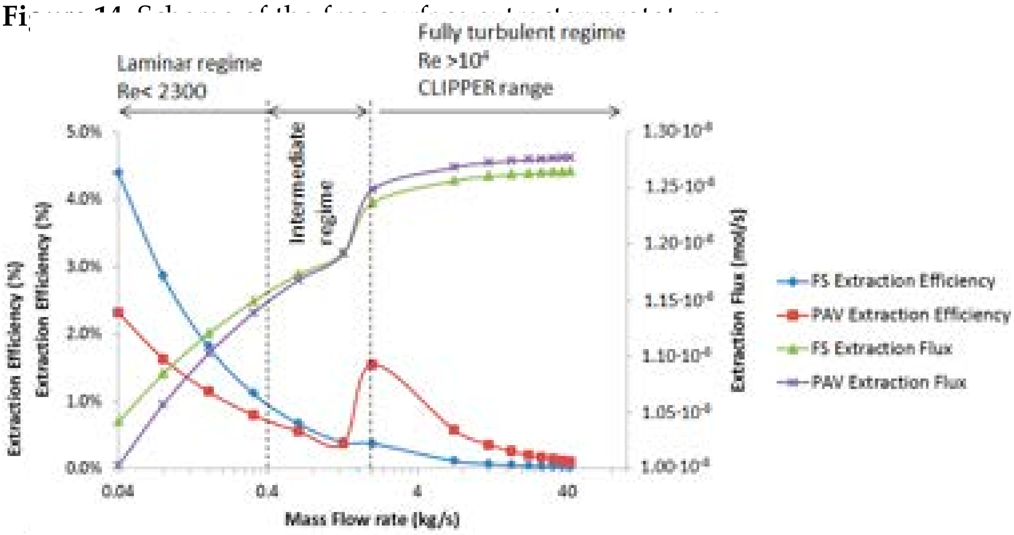

Figure 15. The extraction efficiency and extraction flux as functions of the mass flow rate (FS: free surface; PAV: with membrane) [25].

3.3.2. LVC Design for DEMO

A preliminary conceptual design for the free surface LVC for DEMO was evaluated under the EUROfusion FP9 framework. The operating conditions adopted for the design are reported in Tables 1 and 2. In the preliminary conceptual design, a set of tritium extraction units n_{TEU} (-) are considered for each LiPb loop, and each TEU is composed of n_{ch} (-) number of rectangular channels of width w_{ch} (m) and height r_{ch} (m), with a total length H (m), where the LiPb flows at velocity v (m s^{-1}). The LiPb is distributed on all w_{ch} and only partially fills the channel with a height of r_{LiPb} (m). The remaining part is filled by the vacuum domain. The sizing was carried out considering different channel widths w_{ch}, and the total length H was found from an iterative calculation that ensured reaching the target efficiency of 80%. The equations exploited for the analysis are reported in [11,31]. Tritium transport in the free surface LVC is described by the parameter $C = \frac{K_t}{K_r}\frac{1}{c_T}$, which characterizes tritium transport from the bulk of the liquid towards the vacuum. When $C \ll 1$, the mass transfer in the liquid is the slowest phenomenon and the transport regime is liquid-limited (LLR). If $C \gg 1$, the transport regime is limited by recombination at the liquid–vacuum interface or in the surface-limited regime (SLR). The channel height was chosen as a trade-off between the LiPb flow rate and having a thin LiPb thickness to facilitate tritium extraction. The analysis was mainly performed as a preliminary evaluation of the size of an LVC-type system.

In Figure 16, the total length of the channel required to reach the target efficiency of 80% is shown (left y-axis) as a function of K_r for the OB at 500 °C (left) and 330 °C (right). On the right axis, the corresponding C value is presented. The recombination constant

LiPb thickness to facilitate tritium extraction. The analysis was mainly performed as a preliminary evaluation of the size of an LVC-type system.

In Figure 16, the total length of the channel required to reach the target efficiency of 80% is shown (left y-axis) as a function of K_r for the OB at 500 °C (left) and 330 °C (right). On the right axis, the corresponding C value is presented. The recombination constant

has been swept between $1 \cdot 10^{-2}$ and $1 \cdot 10^{2}$ times the reference value reported in Table 7. In addition, the channel width has been changed to between 1 and 4 m. It is evident that the recombination coefficient has a strong impact on the required dimension of the system, which decreases as the K_r increases, and the same consideration is valid when increasing the channel width. For the reference recombination constant (highlighted by the black vertical line) and for $w_{ch} = 4$ m at 500 °C, the length of the channel becomes 16 m (efficiency 80.2%) compared to 61 m in the case of $w_{ch} = 1$ m. With the reference transport properties, the resulting C at the inlet of the system is 2.66, meaning that the regime is intermediate between surface-limited and liquid-limited. For the smaller K_r, the regime is surface-limited. Moving to the higher K_r, the effect of the recombination constant on the solution becomes smaller as the regime becomes closer to the LLR. For the 330 °C case, the size of the system increases, and the length of the channel becomes 58 m for $w_{ch} = 4$ and 231 m for $w_{ch} = 1$. An analogous activity was performed by changing the K_t, showing a big dependence of the size of the extractor on this parameter. This analysis is justified by the fact that the K_t value found in [10] is an empirical value derived for static PbLi. Therefore, there is significant uncertainty in the value of K_t, and indeed a higher value than the one reported in Table 2 is expected for pressure-driven flows such as the ones of the FS LVC.

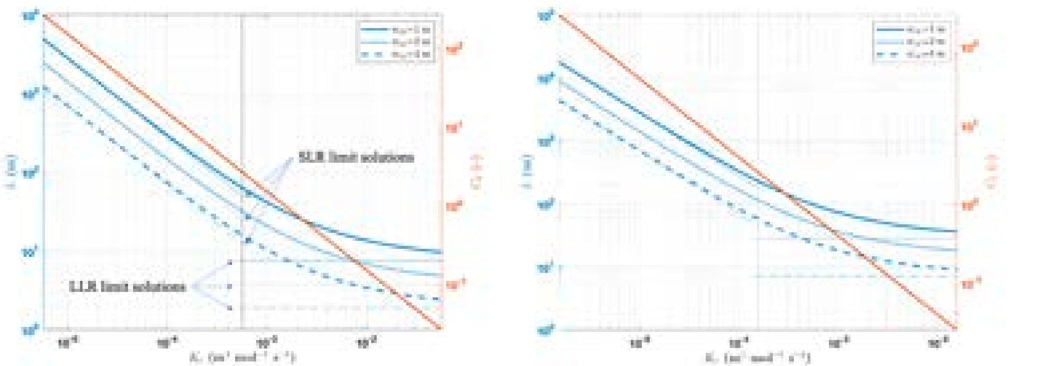

Figure 16. Channel length required to reach 80% efficiency for the LVC design as a function of K_r and w_{ch} for the OB TEU at 500 °C (**left**) and 330 °C (**right**).

In Table 8, the results of the preliminary sizing are reported. The analysis highlighted the necessity to have reliable tritium transport properties for LiPb, which have a huge impact on the system dimensions. In particular, in recent experimental activities [15], a higher diffusivity with respect to the one proposed by Reiter was obtained. The diffusivity is directly related to the mass transfer coefficient K_t; therefore, a reduction in the required LVC size can be expected.

Table 8. Preliminary sizing results for the free surface LVC for IB and OB segments.

Parameter	OB		IB	
LiPb temperature (°C)	330	500	330	500
Number of TEU, n_{TEU} (-)	6	6	5	5
Channels number, n_{ch} (-)	50	50	50	50
Channel height, (m)	4.00×10^{-2}	4.00×10^{-2}	4.00×10^{-2}	4.00×10^{-2}
LiPb height, r_{LiPb} (m)	1.00×10^{-2}	1.00×10^{-2}	1.00×10^{-2}	1.00×10^{-2}
Channel length, L (m)	58	16	62	17
LiPb/vacuum area, A (m^2)	11,600	3200	12,400	3400

3.4. Comparison among the PAV, GLC, and LVC

Table 9 shows a comparison among the TEUs designed on the basis of the PAVs manufactured with Nb pipes and V plates, the GLC, and the LVC for the LiPb OB loop. The analysis was carried out at 330 °C for one OB LiPb loop.

Table 9. Comparison among TEUs designed for one OB LiPb loop based on the PAV, GLC, and LVC.

Parameter	PAV-Nb Tubes	PAV-V Plates	LVC	GLC
LiPb/Vacuum area, A (m^2)	3723	6840	11,600	-
TEU lenght/height (m)	8	15	58	10
TEU Volume (m^3)	226	34	2784	71
TEU Auxiliary system	Vacuum system and getter system	Vacuum system and getter system	Vacuum system and getter system	Helium line and tritium extraction system from helium
Technology issues	Optimization of Nb pipes shape	Connection between V plates and support structure	Design of LiPb distribution system in order to optimise the interface surface (LiPb–vacuum)	Tritium extraction system from helium

The PAV manufactured with V plates required a higher interface area with respect to the PAV manufactured with Nb tubes but the more compact design reduces the total size of the component. However, the vacuum connection of the V plates with the support structure by welding or using gasket connections is still an open issue to be solved. A better Nb pipe distribution inside the PAV is requested in order to optimize the total volume of the TEU; moreover, particular attention should be dedicated to the welding procedure between the Nb pipes and support plate due to the huge number of pipes, at about 1600 per TEU. The GLC shows a total volume comparable with PAV technologies; moreover, thanks to the high maturity level of the technology there are no manufacturing technological issues, although the system requires an auxiliary system in order to remove the tritium from the stripping gas, with additional hydrogen contents in the range between 0.1 and 0.5% mol. Instead, the PAV and LVC required a vacuum system to extract tritium from LiPb and a getter system able to manage the tritium inventory and for transport to the tritium plant. The LVC requires a huge interface surface between the liquid and vacuum that cannot be obtained with a square channel solution; using the LiPb droplets could be a possible solution but dedicated R&D is requested to investigate the efficiency of the system at a relevant scale from fluid dynamics and tritium extraction point of views.

4. LiPb Purification Systems

The composition of LiPb changes during the reactor operation due to the corrosion of structural materials, the transmutation reactions caused by neutron irradiation, and helium production due to (n, Li) reactions. In order to manage the chemistry of LiPb, three dedicated systems are being designed:

(a) A removal system for activation products;
(b) A removal system for corrosion products;
(c) A removal system for helium solubilized in LiPb.

The irradiation products generated in the LiPb are shown in Table 10(a), while the specific activities after irradiation are summarized in Table 10(b). The most harmful species identified to date are ^3H, Po, and Hg, with specific activity rates after irradiation of 8.89×10^{12}, 2.41×10^{10}, and 5.49×10^{8} Bq/kg, respectively. In order to remove the activated products, a gas saturator plus cold trap was designed. This method is based on collecting metal vapor condensation from a gas that passes through a saturator. The activation products Hg, Po, and ^3H are relatively volatile; therefore, they will be removed by evaporation from the hot liquid LiPb, as shown in Figure 17. The base of the saturator is a spray column with a liquid distributor located at the top. Here, the liquid will pass through a set of 1 mm nozzles. Drops will fall through a column of gas into a collecting tank at the bottom. The falling height will be approximately 1 m.

tank at the bottom. The falling height will be approximately 1 m.

Table 10. LiPb activation products and specific activity.

(a) Activated Products Generated in LiPb			**(b) Specific Activities after Irradiation**		
Reactant	**Reaction Type**	**Products**	**Species**	**Half Time**	**Specific Activity after Irradiation [Bq/kg]**
^{6}Li	n, T	^{3}H, ^{4}He	^{3}H	12.32 y	8.89×10^{12}
^{7}Li	n, 2n	^{6}Li	^{203}Hg	46.6 d	2.41×10^{10}
^{7}Li	n, γ	^{8}Li	^{204}Tl	3.78 y	6.91×10^{9}
^{7}Li	n, d	^{6}He	^{202}Tl	122.2 d	1.16×10^{9}
^{204}Pb	n, n′	^{204m}Pb	^{210}Po	138 d	5.49×10^{8}
^{204}Pb	n, 2n	^{203}Pb	^{203}Pb	51.9 h	2.37×10^{7}
^{204}Pb	n, γp	^{204}Tl	^{210}Bi	5.01 d	5.86×10^{6}
^{206}Pb	N, T	^{204}Tl	^{205}Pb	1.5×10^{7} y	4.61×10^{6}
^{206}Pb	N, α	^{203}Hg	^{207}Bi	32.2 y	6.95×10^{5}

Moreover, in the WCLL BB, the LiPb activation is also due to the corrosion products activated by the neutron flux. Therefore, strategies to mitigate corrosion and remove the corrosion product have to be conceived and put into practice. The main corrosion products for these steels are chromium, iron, and manganese [32].

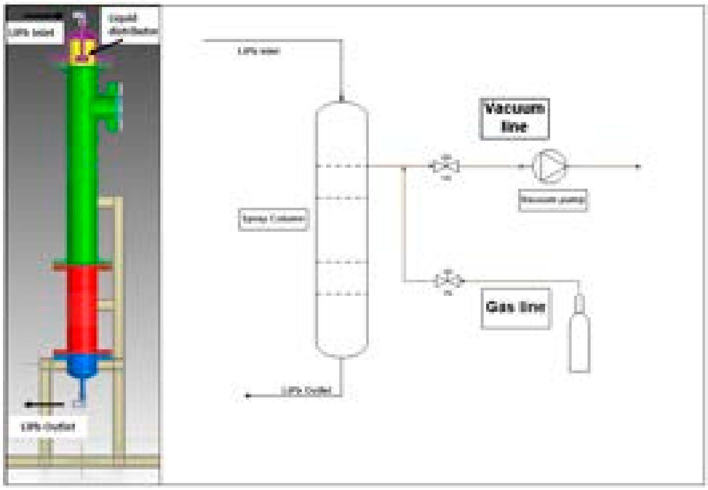

Figure 17. P&ID and schematic view of the system for the removal of the activation product.

The low LiPb velocity and temperature do not foster corrosion but the large surface of the entire system causes the amount of corrosion products to be large enough to require a removal system. Indeed, corrosion products can hinder the correct operation of the loops by forming plugs caused by precipitation in cold spots, near discontinuities, or where the magnetic field is more intense. The reference values of impurities in the LiPb must fulfill the following requirements [31,33]:

- The Li content must be in the range of 15.7 ± 0.5 at%, i.e., 0.62 ± 0.03 wt%;
- Ag, Cu, Nb, Pd, and Zn should be less than 0.001 wt% each;
- Fe, Cr, Mn, Mo, Ni, and V should be less than 0.005 wt% each;
- Si and Al should be less than 0.01 wt% each;
- Bi, Sn, and W should be less than 0.02 wt% each.

The common approach in order to avoid the precipitation of corrosion products is to control the liquid metal's chemistry by purifying the liquid metal.

The purification system used in fission procedures and applied also to TER is essentially composed of a cold trap (CT) [34] consisting of a heat and mass transfer device. The principle of the *CT* is to maintain the impurity equilibrium concentration in the loop below the LiPb solubility at the lowest temperature (T_{low}) foreseen in the plant ($T_{ct} < T_{low}$). The corrosion products and impurities precipitated in the solid state are removed, avoiding the precipitation in the loop. For a generic solute or solvent system with a source term S g/s, the impurity concentration *C(t)*, in ppm, can be obtained from a balance equation:

$$C(t) = C^{\infty}\left(1 - e^{\frac{\eta\, \dot{m}_{ct}}{M} t}\right) \tag{3}$$

where M is the LiPb total mass in the system (kg), $\dot{m}_{ct}$ is the mass flow in the *CT*, η is the *CT* efficiency, and C^{∞} is the asymptotic concentration (t → ∞), defined as:

$$C^{\infty} = \left(\frac{S}{\eta\, \dot{m}_{ct}} + C_{ct}^{Sat}\right) \tag{4}$$

where C_{ct}^{Sat} represents the iron solubility at the minimum *CT* temperature, T_{ct} (with iron being the main component of F/M steel). Concerning the *CT* efficiency, it can be generically defined as:

$$\eta = \frac{C_{in} - C_{out}}{C_{in} - C_{ct}^{Sat}} \tag{5}$$

In an initial assessment, it is assumed to have the same form of *CT* efficiency defined for the sodium purification system:

$$\eta = \frac{1}{1 + p\, \tau^{q}} \tag{6}$$

where τ represents the fluid residence time (min) in the *CT* and p and q are coefficients set as equal to 122 and 3.4, respectively, for sodium *CT*. The appropriateness of such a correlation for the LiPb corrosion system should be evaluated experimentally with a chemical analysis of LiPb sampling upstream and downstream of the *CT*. Referring to the schematic of Figure 18, the following thermal balance can be written:

$$\dot{m}_{ct}\, \bar{c}_p (T_i - T_{ct}) = \dot{m}_T \bar{c}_p (T_i - T_0) \tag{7}$$

then:

$$\dot{m}_{ct} = \dot{m}_T \frac{(T_i - T_0)}{(T_i - T_{ct})} \tag{8}$$

From Equation (8), it is possible to derive the mass flow rate repartition through the *CT*.

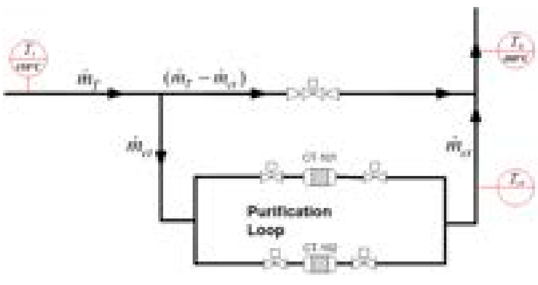

Figure 18. Mass flow rate repartition and temperatures.

Finally, once the residence time and mass flow rate through the *CT* are fixed through Equation 8, it is possible to derive the volume of the *CT*:

$$V_{ct} = \tau \cdot 60 \cdot \dot{m}_T \cdot \rho \cdot \frac{T_i - T_0}{T_i - T_{ct}} \tag{9}$$

A scheme of the purification system is shown in Figure 19.

Finally, once the residence time and mass flow rate through the *CT* are fixed through Equation 8, it is possible to derive the volume of the *CT*:

$$V_{ct} = \tau \cdot 60 \cdot \dot{m}_T \cdot \rho \cdot \frac{T_i - T_0}{T_i - T_{ct}} \tag{9}$$

A scheme of the purification system is shown in Figure 19.

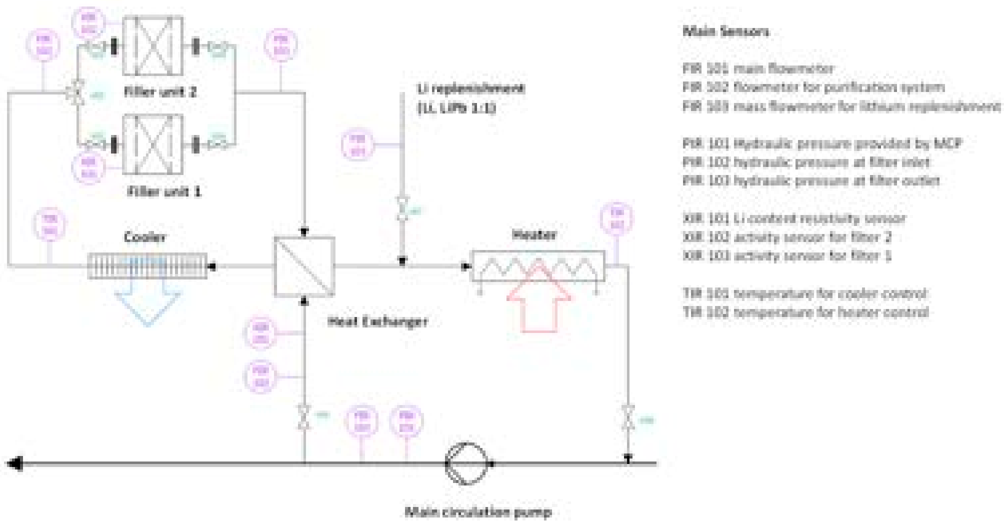

Figure 19. Details of the purification system.

The incoming LiPb then passes through a regenerative heat exchanger and an additional cooler to reach the temperature of 250 °C. The cooled LiPb is then led into a set of two filtering units. The redundancy is needed to ensure the continuous operation of the system even when a unit is plugged. The condition of each unit is monitored by a differential pressure transducer; when the measured pressure drops increase above a threshold, the filtering unit needs to be cleaned. After passing through the cold traps, the LiPb is reheated in a regenerative heat exchanger and in a dedicated heater before re-entering into the main loop. The available experimental data on the corrosion rate for ferritic–martensitic steels in flowing LiPb show a large dispersion, predicting values at high temperatures (450–500 °C) ranging from 5 μm/y to a few hundred μm/y [32,35]. A preliminary design of the CT was carried out with a conservative approach [36], where the CT is composed of a set of bayonet tubes and each bayonet is in turn composed of:

- An outer pipe, DN 1″ (De 33.4 mm × 3.38 mm);
- A middle pipe, DN 1″ (De 25.4 mm × 2.11 mm);
- An inner pipe, DN 5/8″ (De 15.88 mm × 1.24 mm).

The volume between the outer and middle pipes (annulus) is filled with stainless steel powder to reduce the thermal stress across the pipe thickness (Figure 20). Moreover, the bayonet configuration allows the complete disassembly of the tubes from the shell side for maintenance in case of plugging of the CT.

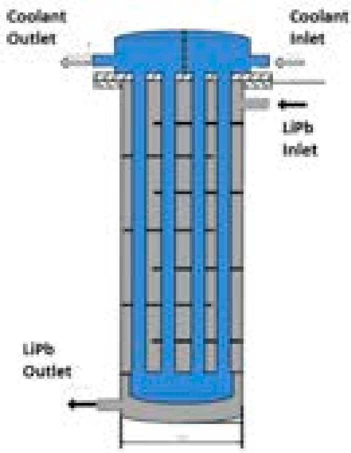

Figure 20. Cold trap layout.

The system devoted to removing the activated products with a gas satura
cold trap should be placed in the upper part of the system within the buffer tank
is used also to ensure the discharge of the helium bubbles generated in the BB. Ab
g of helium is generated daily by the lithium absorption of neutrons:

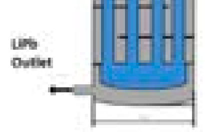

Figure 20. Cold trap layout.

The system devoted to removing the activated products with a gas saturator plus cold trap should be placed in the upper part of the system within the buffer tank, which is used also to ensure the discharge of the helium bubbles generated in the BB. About 500 g of helium is generated daily by the lithium absorption of neutrons:

$$Li_3^6 + n \rightarrow H^3 + He^4 \quad (10)$$

This amount of helium coalesces to form bubbles, which in the WCLL BB have a flow range of about 10–40 mL/h [12]. Helium must be removed from LiPb to avoid its accumulation, which would create local spots where the structure is not cooled. The capability of helium to form bubbles depends on the LiPb mass flow rate, temperature, and pressure. The last two directly influence the helium solubility in LiPb, while the former sets the LiPb residence time in the BB or in the removal system. The longer the time spent in the breeding blanket, the greater the amount of helium generated in a certain volume of LiPb. The longer the time spent in the removal system, the greater the amount of helium released.

Therefore, helium can be removed from LiPb, reducing its velocity and pressure. These conditions are met in the expansion tank, Figure 21, which is the component at the highest level, thereby having the lowest pressure of the entire system. The LiPb velocity has to be reduced in the expansion tank to about 10–15 mm/s (depending on the helium bubble size). Taking into account that the tank will be placed horizontally in order to lengthen the LiPb path inside it, we designed only one tank that hosts the LiPb pumping system and works as an expansion and helium extraction tank.

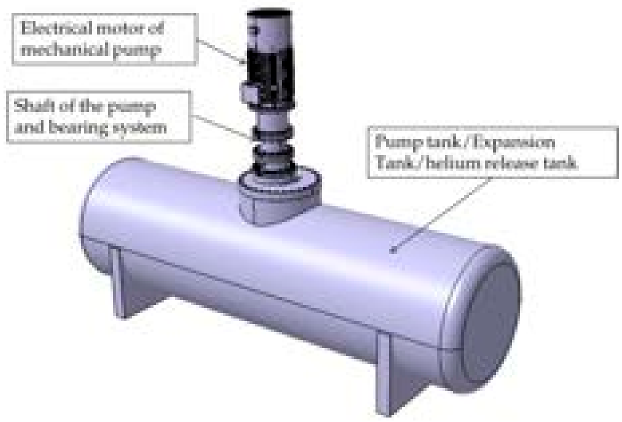

Figure 21. Helium release, expansion, and pumping tank.

5. LiPb Pumping System

To circulate the liquid metal through the BB, a pumping system was designed based on mechanical centrifugal pump technology, which was selected as the reference solution instead of a permanent magnet pump due to its higher efficiency range (50÷60% instead of 7%). The design of the pumps was carried out under the operating conditions of IB and OB loops, based on the required volumetric flow rates and pressure head identified by two operating points, i.e., the part-load point (PLP) and best efficiency point (BEP). Table 11 shows the target performance of the pump.

Table 11. Operating parameters of the pump.

	Q	**H**
	[m^3/h]	**[m]**
PLP	30.4	30.0
BEP	72.9	15.0

Table 11. Operating parameters of the pump.

	Q [m^3/h]	H [m]
PLP	30.4	30.0
BEP	72.9	15.0

Considering a reference temperature T_{ref} range of between 300.0 and 350.0 °C, the maximum pump rotating speed is fixed at 1450.0 rpm, which will vary when using an inverter to fit the best results in terms of the head capacity and power consumption. The model, from a general point of view, is classified at the design point "BEP" as a pure radial pump according to Cordier's diagram. Figures 22 and 23 show the flow domain of the pump, coupling the velocity profiles with the static pressure behavior; it is evident that there is a natural peak of velocity near the tongue of the volute, with no inlet separation or shock being shown. Moreover, the evolution of the pressure profile on the impeller hub and blades does not denote flow separation along the meridian coordinate *m*.

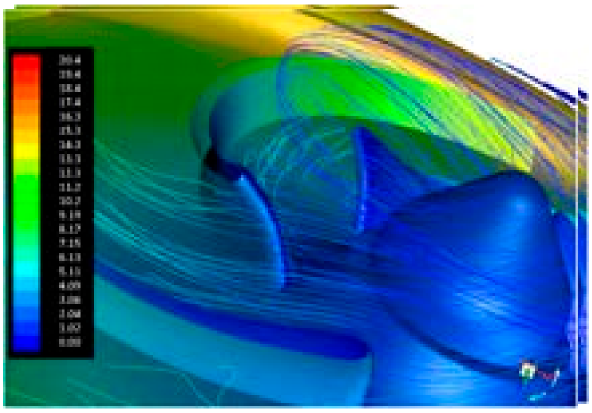

Figure 22. Impeller blade inlet (velocity in m/s).

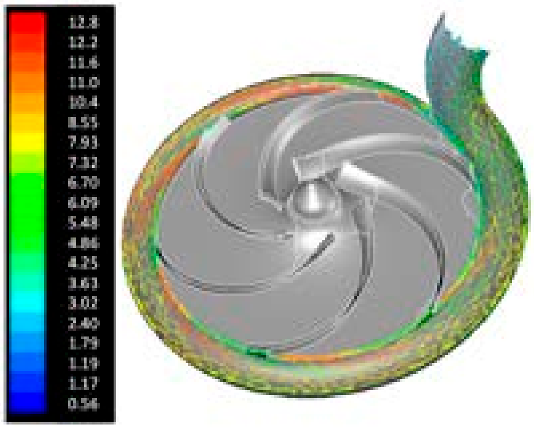

Figure 23. Absolute velocity on the volute (velocity in m/s).

The hydraulic analysis we carried out allowed us to determine the main characteristic of the pumps:

- Rotational speeds: 1000 rpm (for outboard), 750 rpm (for inboard);
- Efficiency η = 60%;
- Hydraulic power with LiPb: 48 kW (outboard), 40 kW (inboard);
- Electric motor required: 90 kW, 6 poles.

The main seal of the pump is located in the oiled bearing frame. It consists of a seal with a magnet drive (Figure 24). The external magnet is mechanically coupled to the electric motor, while the internal magnet is coupled to the shaft. When the motor runs, the shaft rotates as a result of the magnetic field created by the two magnets. Between the external and internal magnets there is a rear casing, which has the function of keeping the liquid in the pump.

liquid in the pump.

The oil used to lubricate the balls in the bearing frame and in the radial bearing and to cool the shaft is discharged from the first compartment of the sealed frame.

If, for any reason, the oil does not discharge from the first compartment, it is drained from the second vane. In this way, it is not possible for the LiPb to come into contact with the oil and with the upper part of the pump. The pump's characteristic curves are shown in Figure 25.

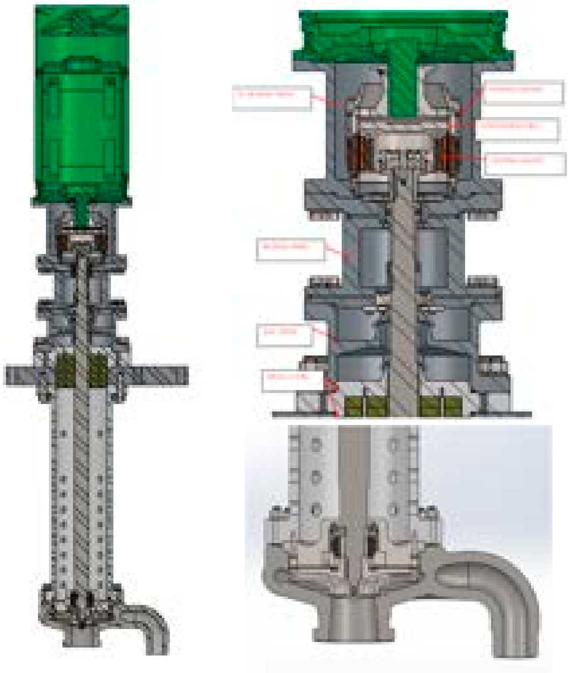

Figure 24. Cross-sectional drawing of the pump.

Figure 24. Cross-sectional drawing of the pump.

The oil used to lubricate the balls in the bearing frame and in the radial bearing and to cool the shaft is discharged from the first compartment of the sealed frame.

If, for any reason, the oil does not discharge from the first compartment, it is drained from the second vane. In this way, it is not possible for the LiPb to come into contact with the oil and with the upper part of the pump. The pump's characteristic curves are shown in Figure 25.

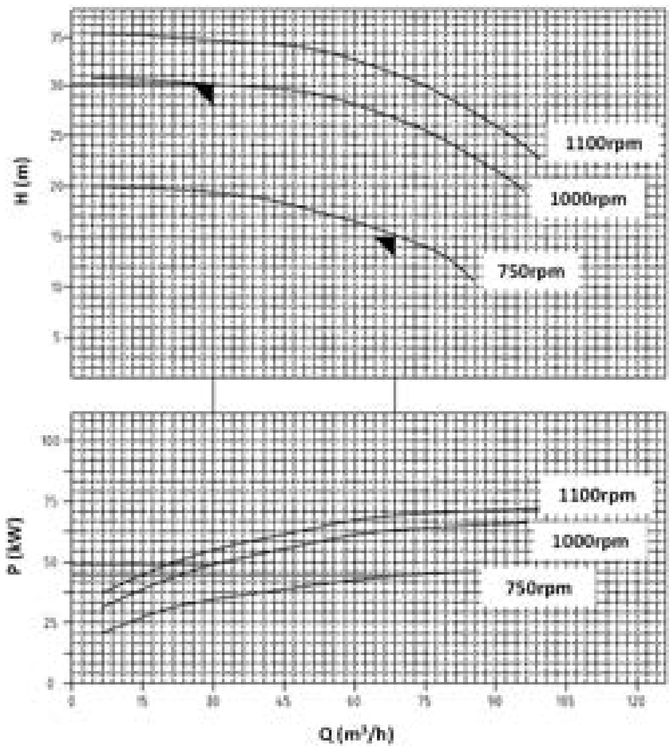

Figure 25. Characteristic curves for the main pumping system.

Figure 25. Characteristic curves for the main pumping system.

6. TER Integration in the Tokamak Building

The TER loops have to be integrated into the tokamak building while taking into account certain technical issues. First of all, the TEU must be placed as close as possible to the outlet from the BB in order to reduce the tritium concentration in the loop and tritium leakage into the environment. In order to allow the integration of the PAV or GLC, the

6. TER Integration in the Tokamak Building

The TER loops have to be integrated into the tokamak building while taking into account certain technical issues. First of all, the TEU must be placed as close as possible to the outlet from the BB in order to reduce the tritium concentration in the loop and tritium leakage into the environment. In order to allow the integration of the PAV or GLC, the reserved space considers the dimensions of the biggest component. The gravitational draining of the BB, the pipework, and the LiPb equipment shall be assured by placing the storage tank in the lowest part of the loops and routing the LiPb pipes to it with a slope of at least 3°.

According to the assumed requirements, the main components of the loops were placed at floor level 3 in one dedicated area to perform the shielding and tritium con- …d by concrete walls with a

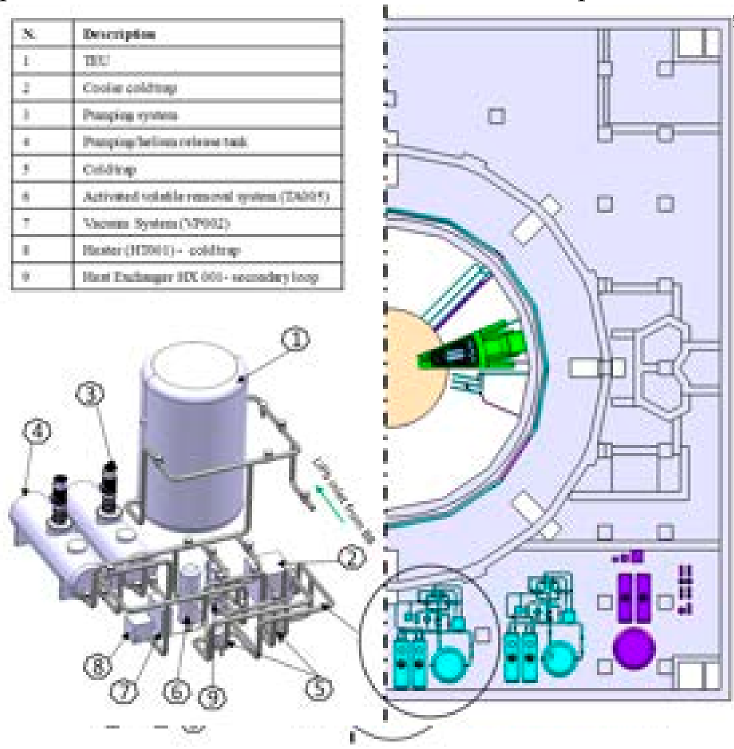

Figure 26. TER integration into the tokamak building.

Figure 26. TER integration into the tokamak building.

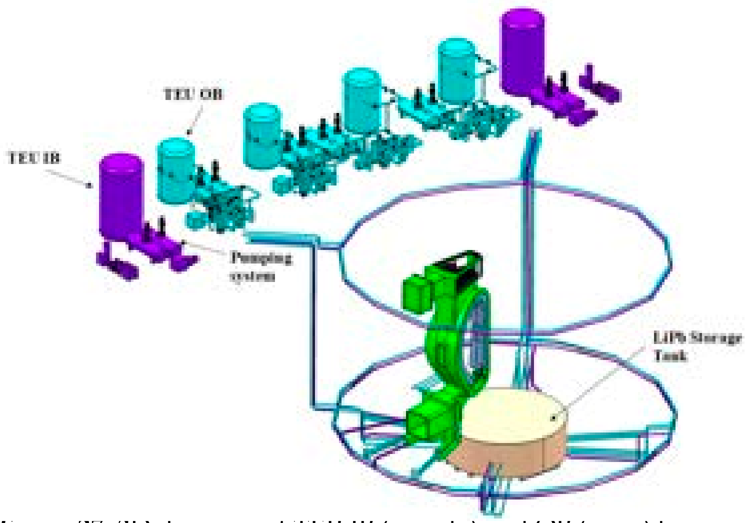

Figure 27. 3D drawing of TER IB (purple) and OB (cyan) loops.

Figure 27. 3D drawing of TER IB (purple) and OB (cyan) loops.

7. Conclusions

7. Conclusions

The preliminary design of TER LiPb loops was completed, including the design of a TEU based on the PAV and GLC. In order to select the best technologies, dedicated experimental R&D is mandatory to support the modelling of the TEU. In particular, the major concerns are related to the tritium transport coefficients. The PAV technology shows

The TEU concept integrated here is based on PAV technology manufactured and with Nb tubes, and the space reserved is enough to allocate a TEU based on GLC technology if selected as the reference solution.

7. Conclusions

The preliminary design of TER LiPb loops was completed, including the design of a TEU based on the PAV and GLC. In order to select the best technologies, dedicated experimental R&D is mandatory to support the modelling of the TEU. In particular, the major concerns are related to the tritium transport coefficients. The PAV technology shows some advantages over the GLC from the point of view of the operation and auxiliary system required, as in the PAV the tritium is directly extracted by the vacuum system and can be stored by a getter system before being transferred with the support of purge gas to the tritium processing plant. Instead, tritium extracted by GLCs is mixed with helium, and if a mix of helium and hydrogen is used as the stripping gas with protium (H2, T2, HT), a dedicated tritium extraction system from helium fluxes in the range of 100–6000 Nm3/h is required. In order to select the best TEU technology for the WCLL BB, several parameters have to be evaluated, such as the technology readiness level (TRL), manufacturing process, integrability, reliability, operability, remote maintenance procedures, waste management procedures, and costs. The selection procedure must also take into consideration the auxiliary circuits required to operate the TEU, vacuum system, and getter for the PAV/LVC and the tritium extraction system from helium for the GLC. Moreover, if the GLC is selected, it can be used also for helium removal from LiPb, meaning it will be possible to reduce the size of the expansion tank used as the helium removal system. To validate the PAV design, R&D activities are required to analyze how the membrane materials' permeability is affected by the superficial status of the membrane. A TEU based on PAV technology and designed with a surface permeation regime was integrated into the tokamak building together with the other auxiliary systems (chemistry control system, pumping system, storage tank, etc.), taking into account the safety requirements (e.g., tritium release into environment, shielding of the systems, accidental scenarios) and remote maintenance requirements. A preliminary design of the system devoted to removing the corrosion-activated products was completed to control the impurity concentration in the liquid metal. Dedicated R&D is required in order to validate the solution proposed to remove helium in the expansion tank of LiPb and control the LiPb's chemistry in order to validate the codes under development. A mechanical pump with a magnetic bearing was designed in order to circulate the LiPb IB and OB mass flows outside the BB and into the tank used to remove the helium solubilized from LiPb. The 3D drawings of the LiPb loops were completed by considering the main interfaces between the loops and the other systems and their integration in the tokamak building.

Author Contributions: Conceptualization, M.U. and D.R.; Software, R.M.; Validation, M.K. and F.R.U.; Investigation, C.A., R.B., L.C., A.C., B.G., D.M., F.P. and L.S.; Data curation, D.V.; Writing—original draft, M.U.; Supervision, A.V. All authors have read and agreed to the published version of the manuscript.

Funding: This research was funded by European Union via the Euratom Research and Training Programme (Grant Agreement No 101052200—EUROfusio), partially funded by the MINECO Ministry under project ENE2013- 43650-R and by Community of Madrid, co-financed with Structural Funds (ERDF and ESF)), through the TechnoFusión (III)-CM (S2018/EMT-4437) programme.

Data Availability Statement: Not applicable.

Conflicts of Interest: The authors declare no conflict of interest.

References

1. Cismondi, F.; Spagnuolo, G.; Boccaccini, L.; Chiovaro, P.; Ciattaglia, S.; Cristescu, I.; Day, C.; Del Nevo, A.; Di Maio, P.; Federici, G.; et al. Progress of the conceptual design of the European DEMO breeding blanket, tritium extraction and coolant purification systems. *Fusion Eng. Des.* **2020**, *157*, 111640. [CrossRef]
2. Martelli, D.; Venturini, A.; Utili, M. Literature review of lead-lithium thermophysical properties. *Fusion Eng. Des.* **2018**, *138*, 183–195. [CrossRef]
3. Demange, D.; Antunes, R.; Borisevich, O.; Frances, L.; Rapisarda, D.; Santucci, A.; Utili, M. Tritium extraction technologies and DEMO requirements. *Fusion Eng. Des.* **2016**, *109–111*, 912–916. [CrossRef]
4. Tahara, A.; Hayashi, Y. Measurements of Permeation of Hydrogen Isotopes through α-Iron by Pressure Modulation and Ion Bombarding. *Trans. Jpn. Inst. Met.* **1985**, *26*, 869–875. [CrossRef]
5. Okino, F.; Calderoni, P.; Kasada, R.; Konishi, S. Feasibility analysis of vacuum sieve tray for tritium extraction in the HCLL test blanket system. *Fusion Eng. Des.* **2016**, *109–111*, 1748–1753. [CrossRef]
6. Okino, F.; Noborio, K.; Kasada, R.; Konishi, S. Enhanced Mass Transfer of Deuterium Extracted from Falling Liquid Pb-17Li Droplets. *Fusion Sci. Technol.* **2013**, *64*, 543–548. [CrossRef]
7. Cantore, M. Qualification of Tritium Extraction System from Pb15.7Li in TRIEX-II Facility. Available online: https://webthesis.biblio.polito.it/11312/1/tesi.pdf. (accessed on 1 January 2020).
8. Utili, M.; Alberghi, C.; Candido, L.; Papa, F.; Tarantino, M.; Venturini, A. TRIEX-II: An experimental facility for the characterization of the tritium extraction unit of the WCLL blanket of ITER and DEMO fusion reactors. *Nucl. Fusion* **2022**, *62*, 066036. [CrossRef]
9. Aiello, A.; Ciampichetti, A.; Benamati, G. Determination of hydrogen solubility in lead lithium using sole device. *Fusion Eng. Des.* **2006**, *81*, 639–644. [CrossRef]
10. Reiter, F. Solubility and diffusivity of hydrogen isotopes in liquid PbLi. *Fusion Eng. Des.* **1991**, *14*, 207–211. [CrossRef]
11. Terai, T. Mass Transfer Coefficient of Tritium from Molten Lithium-Lead Alloy (Li17Pb83) to Environmental Gas under Neutron Irradiation. *Fusion Eng. Des.* **1991**, *17*, 237–247. [CrossRef]
12. Pisarev, A.; Tanabe, T.; Terai, T.; Benamati, G.; Mullin, M. Modeling of In-Pile Experiments on Tritium Release from Molten Lithium-Lead. *J. Nucl. Sci. Technol.* **2012**, *39*, 377–381. [CrossRef]
13. Garcinuño, B.; Rapisarda, D.; Fernández-Berceruelo, I.; Jiménez-Rey, D.; Sanz, J.; Moreno, C.; Palermo, I.; Ibarra, A. Design and fabrication of a Permeator Against Vacuum prototype for small scale testing at Lead-Lithium facility. *Fusion Eng. Des.* **2017**, *124*, 871–875. [CrossRef]
14. Garcinuño, B.; Rapisarda, D.; Fernández, I.; Moreno, C.; Palermo, I.; Ibarra, A. Design of a permeator against vacuum for tritium extraction from eutectic lithium-lead in a DCLL DEMO. *Fusion Eng. Des.* **2017**, *117*, 226–231. [CrossRef]
15. Papa, F.; Utili, M.; Venturini, A.; Caruso, G.; Savoldi, L.; Bonifetto, R.; Valerio, D.; Allio, A.; Collaku, A.; Tarantino, M. Engineering design of a Permeator against Vacuum mock-up with niobium membrane. *Fusion Eng. Des.* **2021**, *166*, 112313. [CrossRef]
16. Bonifetto, R.; Utili, M.; Valerio, D.; Zanino, R. Conceptual design of a PAV-based tritium extractor for the WCLL breeding blanket of the EU DEMO: Effects of surface-limited vs. diffusion-limited modelling. *Fusion Eng. Des.* **2021**, *167*, 112363. [CrossRef]
17. Anderson, T.L. Evaluation of the Corrosion Resistance of 2 1/4 Cr-1 Mo Steel in a Lithium–Lead Liquid. Master's Thesis, Colorado School of Mines, Illinois, CO, USA, 1980.
18. Malo, M.; Peñalva, I.; Azkurreta, J.; Garcinuño, B.; Liu, H.-D.; Rapisarda, D.; Zhou, H.-S.; Luo, G.-N. Experimental refutation of the deuterium permeability in vanadium, niobium and tantalum. *Fusion Eng. Des.* **2019**, *146*, 224–227. [CrossRef]
19. Steward, S.A. Review of Hydrogen Isotope Permeability through Materials, Tech. Rep., Lawrence Livermore National Laboratory. 1983. Available online: http://www.osti.gov/servlets/purl/5277693/ (accessed on 15 August 1983).
20. Garcinuño, B.; Rapisarda, D.; Moreno, C.; Sanz, J.; Ibarra, A. Design of a System for Hydrogen isotopes Injection into Lead-Lithium. *Fusion Eng. Des.* **2018**, *137*, 427–434. [CrossRef]
21. Garcinuño, B.; Rapisarda, D.; Fernández-Berceruelo, I.; Carella, E.; Sanz, J. The CIEMAT PbLi Loop Permeation Experiment. *Fusion Eng. Des.* **2019**, *146*, 1228–1232. [CrossRef]
22. Urgorri, F.R.; Moreno, C.; Carella, E.; Castellanos, J.; Del Nevo, A.; Ibarra, Á. Preliminary system modelling for the EUROfusion water cooled lithium–lead blanket. *Fusion Sci. Technol.* **2017**, *71*, 444–449. [CrossRef]
23. Garcinuño, B.; Rapisarda, D.; Antunes, R.; Utili, M.; Fernández-Berceruelo, I.; Sanz, J.; Ibarra, A. The tritium extraction and removal system for the DCLL-DEMO fusion reactor. *Nucl. Fusion* **2018**, *58*, 095002. [CrossRef]
24. Urgorri, F.; Garcinuño, B.; Moreno, C.; Rapisarda, D. Theoretical evaluation of the tritium extraction from liquid metal flows through a free surface and through a permeable membrane. *Nucl. Fusion* **2023**, *63*, 046025. [CrossRef]
25. Green, D.W.; Perry, R.H. Equipment for distillation, gas absorption, phase dispersion and phase separation. In *Perry's Chemical Engineers Handbook*; McGraw-Hill: New York, NY, USA, 2008.
26. Spagnuolo, G.A.; Arredondo, R.; Boccaccini, L.V.; Coleman, M.; Cristescu, I.; Federici, G.; Franza, F.; Garcinuño, B.; Moreno, C.; Rapisarda, D.; et al. Integration issues on tritium management of the European DEMO Breeding Blanket and ancillary systems. *Fusion Eng. Des.* **2021**, *171*, 112573. [CrossRef]
27. Richardson, J.F.; Harker, J.H.; Backhurst, J.R. Separation Columns (Distillation, Absorption and Extraction). In *Coulson and Richardson's Chemical Engineering*; Butterworth-Heinemann: Oxford, UK, 2005.

28. Spagnuolo, G.; Arredondo, R.; Boccaccini, L.; Chiovaro, P.; Ciattaglia, S.; Cismondi, F.; Coleman, M.; Cristescu, I.; D'Amico, S.; Day, C.; et al. Integrated design of breeding blanket and ancillary systems related to the use of helium or water as a coolant and impact on the overall plant design. *Fusion Eng. Des.* **2021**, *173*, 112933. [CrossRef]
29. Garcinuño, B. H-isotopes extraction from liquid PbLi using permeation against vacuum: Permeable membrane vs. free-surface. In Proceedings of the 7th International Symposium on Liquid Metals Applications for Fusion (ISLA-7), Aichi, Japan, 12–17 December 2022.
30. Malo, M.; Peñalva, I.; Azkurreta, J.; Garcinuño, B.; Liu, H.-D.; Rapisarda, D.; Zhou, H.-S.; Luo, G.-N. Experimental Determination of Hydrogen Isotope Transport ParameTER in Vanadium. *Membranes* **2022**, *12*, 579. [CrossRef] [PubMed]
31. Alberghi, C.; Candido, L.; Utili, M.; Zucchetti, M. Development of new analytical tools for tritium transport modelling. *Fusion Eng. Des.* **2022**, *177*, 113083. [CrossRef]
32. Martelli, D.; Bassini, S.; Utili, M.; Tarantino, M.; Lionetti, S.; Zanin, E. LIFUS II corrosion loop final design and screening of an Al based diffusion coating in stagnant LLE environment. *Fusion Eng. Des.* **2020**, *160*, 112034. [CrossRef]
33. Garcinuño, B.; Fernández-Saavedra, R.; Hernández, T.; Gomez, M.B.; Quejido, A.; Rapisarda, D. Establishing technical specifications for PbLi eutectic alloy analysis and its relevance in fusion applications. *Nucl. Mater. Energy* **2022**, *30*, 101146. [CrossRef]
34. Kordač, M.; Košek, L. Helium bubble formation in Pb-16Li within the breeding blanket. *Fusion Eng. Des.* **2017**, *124*, 700–704. [CrossRef]
35. Smolentsev, S.; Saedi, S.; Malang, S.; Abdou, M. Numerical study of corrosion of ferritic/martensitic steels in the flowing PbLi with and without a magnetic field. *J. Nucl. Mater.* **2013**, *432*, 294–304. [CrossRef]
36. Grundy, B.R. Experimental characterization of sodium Cold Traps and modelling of their behaviour. In Proceedings of the International Conference on Liquid Technology in Energy Production, Champion, PA, USA, 3 May 1976; p. 650.